

# Magnetic field dependence of the atomic and electronic structure of monovalent metallic nanocontacts unveiled in transport experiments

Beilun Wu,<sup>†,‡,¶</sup> Andrés Martínez,<sup>§</sup> Paula Obladen,<sup>†,‡,¶</sup> Marta Fernández-Lomana,<sup>†,‡,¶</sup> Edwin Herrera,<sup>†,‡,¶</sup> Carlos Sabater,<sup>§</sup> Juan José Palacios,<sup>||,‡,¶</sup> Isabel Guillamón,<sup>†,‡,¶</sup> and Hermann Suderow<sup>†,‡,¶</sup>

<sup>†</sup>*Laboratorio de Bajas Temperaturas y Altos Campos Magnéticos, Unidad Asociada UAM-CSIC, Departamento de Física de la Materia Condensada, Universidad Autónoma de Madrid, E-28049 Madrid, Spain*

<sup>‡</sup>*Condensed Matter Physics Center (IFIMAC), Universidad Autónoma de Madrid, E-28049 Madrid, Spain*

<sup>¶</sup>*Instituto Nicolás Cabrera (INC), Universidad Autónoma de Madrid, E-28049 Madrid, Spain*

<sup>§</sup>*Departamento de Física Aplicada and Instituto Universitario de Materiales de Alicante (IUMA), Universidad de Alicante, Campus de San Vicente del Raspeig, E-03690 Alicante, Spain.*

<sup>||</sup>*Departamento de Física de la Materia Condensada, Universidad Autónoma de Madrid, E-28049 Madrid, Spain*

E-mail:

## Abstract

We measure Au and Ag atomic-size contacts in magnetic fields, from zero field to 20 T. We find a magnetic field induced torque which leads to atomic binding at shorter distances than at zero field. Furthermore, the conductance drops below  $G_0$  at high magnetic fields by about 15% in Au. We calculate the conduction through nanosized Au contacts containing residual  $O_2$  molecules attached to the contact region and find a spin polarized current when  $O_2$  is located at the atomic contact. We discuss the role of spin-orbit coupling in the magnetic properties of  $O_2$  attached to Au.

Atomic-size contacts created between two sharp electrodes provide insight into atomic bonding and electronic conduction properties at the nanometric scale.<sup>1-7</sup> The conductance at this scale is mostly coherent and is theoretically well described by Landauer's formula,  $G = G_0 \sum_{i=1}^N T_i$ , where  $G_0 = \frac{2e^2}{h}$  is the quantum of conductance,  $i$  the conduction channel number,  $N$  the number of opened channels and  $T_i$  the quantum transmission through each channel.<sup>8,9</sup>  $N$  and  $T_i$  are related to the valence of the contacting atom.<sup>10</sup> The coefficients  $T_i$  are like a "pin code" characterising the properties of the nanosized conductor.<sup>10</sup> Atomic-size contacts of monovalent Au and Ag exhibit, for example, a conductance plateau at  $G \simeq G_0$  ( $N = 1$  and  $T_1 \approx 1$ ) which is nearly independent on the geometry and shape of the nanocontact.<sup>10-14</sup>

The influence of a magnetic field on the conductance of atomic-size contacts has been considered in Refs.<sup>15-19,19-27</sup> In nanocontacts of Fe and Co, for example, ferromagnetic interactions lead to considerable variations of the conductance  $G$  with magnetic field.<sup>19,26-28</sup> However, most atomic-size contacts presenting features related to the application of a magnetic field are made from elements with a valence which differs from one. Thus, these contacts have several conduction channels,  $N > 1$ , each being only partially open,  $T_i < 1$ . The "pin code" and the conductance through these atomic-size contacts is highly sensitive to the atomic arrangement close to the contact,<sup>13,29</sup> making studies as a function of the magnetic field particularly challenging because of the lack of a well defined reference conductance

value.

Here we examine the question of a possible magnetic response of Au and Ag atomic-size contacts, with studies up to magnetic fields of 20 T. We find that the magnetic field modifies the formation process of the contact in Ag and that there is an increasing number of Au atomic-size contacts with conductance below 15%  $G_0$  at the largest magnetic fields.

We show a representative example of conductance vs distance curves in Au and Ag few atom point contacts at 0 T and at 20 T in Fig. 1. We define  $G_a$ , the conductance just before jumping into contact, and  $G_b$ , the value of the conductance at the first plateau (red and black arrows in Fig. 1).<sup>7,30-34</sup> When looking at isolated conductance vs distance traces, there is no strong and visible effect of the magnetic field at B=20 T. However, as we will show below using histograms made of many traces, the conductance just before the jump to contact,  $G_a$ , increases slightly with the magnetic field, particularly in Ag. Furthermore, the single atom point contact conductance  $G_b$  is smaller than  $G_0$  in some atomic-size point contacts at high magnetic fields, particularly in Au.

To discuss the magnetic field induced effects with more detail, we plot in Fig. 2 histograms of the conductance values  $G_a$  and  $G_b$  as a function of the magnetic field. We find that the value of the maximum in the  $G_a$  histogram,  $G_{a,max}$  is magnetic field dependent, with  $G_{a,max}$  increasing considerably, particularly at the highest magnetic fields and in Ag (Fig. 2). We also find a tail in the histogram with  $G_b < G_0$  at high magnetic fields in Au. This tail is much weaker, if at all present, in Ag for all magnetic fields (Fig. 2).

The value of  $G_{a,max}$  is related to the bonding process between the two atoms at the tip apex. The energy of the two-atom system as a function of the separation between atoms  $z$  can be written as  $E(z) = E_{UBC}(z) + E_{Elastic}(z) + E_{Magnetic}$ . The position of the atoms at the apex is determined by the minimum in  $E(z)$ .  $E_{UBC}(z)$  is the so-called universal binding curve and is given by  $E_{UBC}(z) = \alpha(z - z_0)e^{-\beta(z-z_0)}$ .<sup>35-37</sup> Here,  $z_0$  is the equilibrium bonding distance in absence of any other interaction and  $\alpha$  and  $\beta$  are parameters which we obtain from calculations, described in the Supplementary Information, Section I. From these

parameters, it is seen that the minimum of  $E_{UBC}(z)$ , or the binding energy  $E_0$ , is about 0.8 eV larger in Au than in Ag. Therefore,  $E_{Elastic}(z)$  and  $E_{Magnetic}$  have a much stronger influence in Ag than in Au.

The elastic term  $E_{Elastic}(z) = \frac{k}{2}(D-z)^2$  describes the elastic properties of the nanometric size wires holding the atoms at the tips.<sup>38</sup>  $k$  is the spring constant and  $D$  the length of the spring.  $D$  is externally controlled by changing the position of the electrodes, as discussed with more detail in Supplementary Information Section I.<sup>14,38</sup> There is a considerable spread in  $G_a$ , because the atomic arrangements close to the contact lead to a spread in  $k$ .<sup>38</sup> But  $G_{a,max}$  is higher for Ag than for Au at zero field, because the minimum in  $E(z) = E_{UBC}(z) + E_{Elastic}(z)$  for Au nanocontacts occurs at smaller distances for Ag than for Au, due to the larger  $E_0$  in Au.<sup>30,39</sup>

Under magnetic fields,  $G_{a,max}$  increases in Ag up to a value which is larger than the spread in  $G_a$ . From the variation of  $G_{a,max}$  with field, we estimate that the electrodes come closer by approximately 0.3 Å in Ag (and less than 0.05 Å in Au) when applying a field of 20 T.

The observed magnetic field induced change in  $G_{a,max}$  in Ag shows that  $E_{Magnetic}$  should be of the order of a fraction of an eV. Such values lead to a sizeable modification of the position of the minimum of  $E(z)$  and thus of  $G_{a,max}$  in Ag but not in Au. The anisotropy of the magnetization for parallel and perpendicular field orientations  $\delta\mathbf{M}$  induces a magnetic field dependent torque  $\boldsymbol{\tau} = \delta\mathbf{M} \times \mathbf{B}$ .<sup>40</sup> The torque produces a (rotational) magnetic force and originates the term in the energy balance  $E_{Magnetic}$ . We can write  $E_{Magnetic} \approx \chi_{anis} V \frac{B^2}{\mu_0} \sin(\theta)$ , with  $\theta$  the angle between the magnetization and the magnetic field,  $\chi_{anis} = \chi_{||} - \chi_{\perp}$ , where  $\chi_{||}$  and  $\chi_{\perp}$  are the susceptibilities parallel and perpendicular to the magnetic field and  $V$  the volume over which the torque is acting. For a volume of order of a sphere of radius 100 nm, this implies that  $\chi_{anis} \approx 10^{-4}$ , which is an order of magnitude larger than the bulk. It was shown in Ref.<sup>41</sup> that the anisotropy of the susceptibility of small rods of Au is significantly enhanced with respect to the bulk value, due to mesoscopic circular currents induced by the

magnetic field. Similar effects have been found in both Au and Ag nanoparticles.<sup>42</sup> The role of currents through surface states on rod-like structures was shown to provide an anisotropic susceptibility about an order of magnitude larger than the bulk.<sup>41-43</sup> Therefore, the torque induced by anisotropic surface currents at the leads close to the single atom point contact modifies the energy balance and leads to a magnetic field induced decrease in the position of the minimum of the total binding energy  $E(z)$ . Our data show that there is a sizeable contribution to the binding energy by the magnetic field due to an enhanced anisotropic susceptibility close to the contact region.

On the other hand, the significant number of atomic-size contacts with  $G_b$  below  $G_0$  observed in Au shows that in these contacts the transmission  $T_1$  is reduced below one ( $T_1 < 1$ ) with magnetic field. The transmission is thus magnetic field dependent for some atomic-size contacts.

As we discuss in the Supplementary Information, Section I, neither Au nor Ag have magnetic properties strong enough to have a magnetic response in the conductance of atomic sized contacts  $G_b$ . The experiment is made in cryogenic vacuum conditions, which guarantees that there are strictly no extraneous elements or large molecules in gas phase that can reach the contact area. However, residual air ( $N_2$  and  $O_2$ ) condenses on the sample and might interact with the contact area at some point.  $N_2$  molecules are not magnetic, leaving  $O_2$  as the only magnetically active molecules. The remaining questions are if  $O_2$  molecules can modify electronic conduction through the atomic size contact and how do  $O_2$  molecules reach the contact region.

To analyze this, we first estimate the amount of  $O_2$  residual gas to be approximately  $10^{-7}$  mol. Considering the volume of our experiment, in approximately 10% of the contacts some  $O_2$  molecule could reach the contact area. We note that experimental studies of  $O_2$  contacts required a residual concentration of  $10^{-5}$  mol to obtain sizeable statistics.<sup>44,45</sup> Second, we have to consider that molecules need to be free to move so that some can come close to the contact area in the push pull process that leads to contact formation and breaking. This

implies absent or small reactivity of the metal surface to  $O_2$ . In Ag,  $O_2$  is chemisorbed, so that  $O_2$  molecules are fixed at their positions and the push pull process for contact formation does not move them significantly. However, in Au,  $O_2$  is almost unavoidably physisorbed and has thus a very large mobility.<sup>46</sup> Third, when a  $O_2$  molecule comes close to the contact area, the reactivity increases with the decreasing coordination number of Au,<sup>47,48</sup> and the oxygen is incorporated in the atomic structure at the contact. We conclude that  $O_2$  is free to move around the surface of Au. When it comes close to the sharp apex formed by the push-pull process, it can interact with Au and contribute to the conduction close to the single atom point contact regime.

We have calculated the conduction through atomic-size Au structures including a  $O_2$  molecule at different positions in the vicinity of the single atom point contact. We start with a molecular dynamics simulation of the formation of the nanocontacts (pulling case). We then pick one geometry showing a single atom contact (actually a dimer), add an  $O_2$  molecule on different locations close to it, and relax each case with density functional theory (DFT) (see insets of Fig. 4 and Methods). We finally compute the conductance of the relaxed geometry as a function of the energy. We have performed the calculation at zero field and with an applied field of 20 T along the z direction. The results are shown in Fig. 4.

In atomic-size contacts of Au (before adding the  $O_2$  molecule) we obtain, as expected, that  $G = G_0$  at the Fermi level  $E_F$ , with no sizeable magnetic field dependence (black dashed lines in Fig. 4(a-d) are for zero field and grey dashed lines for 20 T). When adding the molecule, we observe features in the conductance at about 0.5 eV above  $E_F$  and about 1 eV below  $E_F$  in all cases due to the LUMO and HOMO of the molecule (green and yellow dashed lines in Fig. 4(a-d)). These features are slightly shifted with respect to each other under magnetic fields, but the shift does not influence the conductance close to the Fermi energy  $E_F$ .

Notice, however, that the conductance at  $E_F$  does strongly depend on the position of the  $O_2$  molecule. In particular, when  $O_2$  is bonded directly to the two contacting atoms

(Fig. 4(b)), we find a considerable decrease of the conductance below  $G_0$ . The decrease is due to a reduced spin-up current (red line in Fig. 4(b)) and leads to  $G \approx 0.8G_0$  (the magnetic moment of the  $O_2$  molecule at this position is  $1.74 \mu_B$ ).  $G$  shows sizeable differences for spin up and spin down, with a peak quite close to the Fermi level. For other positions of the  $O_2$  molecule, the conductance at the Fermi level remains  $G \approx 0.98G_0$ . In all cases the conductance only slightly changes with the magnetic field (even though the spin remains large, suggesting physisorption instead of chemical interaction, the obtained spin is  $1.21 \mu_B$  in Fig. 4(c) and  $1.3 \mu_B$  Fig. 4(d), as discussed in the Supplementary Information Section II).

The decreased conductance of  $G \approx 0.8G_0$  in the position shown in Fig. 4(b) is similar to what we find in the experiment (a decrease in  $G_b$  by 15% at 20 T). Thus, our calculations show that  $O_2$  indeed leads to spin dependent transport with  $G$  well below  $G_0$  on certain atomic-size contacts. However, note that green zero field and yellow 20 T curves are similar in Fig. 4(b). Thus, it does not explain which such contacts with  $O_2$  appear more often under magnetic fields.

To explain the dependence on the magnetic field, we should consider the influence of the magnetic field in adsorption. The role of spin alignment of  $O_2$  on the adsorption has been considered on reactive metal surfaces, finding a significant influence, as for instance the geometry of the  $O_2$  molecule relative to the surface influences the molecular orbital overlap with the surface (see Refs. <sup>49–55</sup> and Supplementary Information Section II). Our experiment suggests that the sticking is influenced by a magnetic field in nanoscale atomic arrangements of Au. But how can this actually occur?

To address this question, we have estimated the magnetic anisotropy energy (MAE) of the  $O_2$  molecule for a toy model of the contact (see Supplementary Information Section III). We find that Au transfers its large spin orbit coupling (SOC) to the  $O_2$  molecule, giving rise to a sizable MAE value of  $6.5 \cdot 10^{-4}$  eV and a preferred orientation of the magnetic moment in the direction of transport when the  $O_2$  molecule is oriented along that direction, and a smaller MAE of  $8 \cdot 10^{-5}$  eV with a transversal easy axis of magnetization when the  $O_2$

molecule is perpendicular to the contact. This value, along with the favored orientation of the magnetic moment, changes with the position of the molecule. Since the magnetic field is always applied in the same direction, the coupling with the magnetic moment of the molecule favors some physisorption sites over others. Particularly those where  $O_2$  is attached vertically to the contacting atoms, with a magnetic moment parallel to the field (Fig. 4(b)) seem to occur more frequently at high magnetic fields. Thus,  $O_2$  molecules can reach more easily the contacting atoms in the push-pull process of the contact formation in presence of a high magnetic field, leading more frequently to situations with partially spin polarized transport and a conductance of atomic size contacts below  $G_0$ .

In summary, we have measured atomic-size contacts of Ag and Au under magnetic fields up to 20 T. We find a significant influence of the magnetic field in the environment close to the contact. This leads to a modification of the bonding process through the contribution of the magnetic energy due to large anisotropic circulating currents around the leads of the atomic size contact. Furthermore, we reveal a decrease in the transmission of up to about 15% in Au contacts at magnetic fields of 20 T, attributed to  $O_2$  molecules.  $O_2$  molecules present a sizeable MAE due to the spin orbit interaction with Au.

## Methods

### Experimental

We use a cryogenic STM set up with a 20 Tesla fully superconducting magnet from Oxford Instruments.<sup>56</sup> Our STM hardware and software are described in Ref.<sup>57</sup> Au and Ag tips and samples are obtained from wires. To obtain clean and reproducible nanocontacts, we repeatedly indent tip and sample at 4.2 K. This leads to a mechanical annealing of the contact region, described in Refs.<sup>39,58-61</sup> and to the formation of clean and reproducible atomic-size contacts. We use a  $10^6$  current to voltage amplifier with a tip-sample bias voltage of 50 mV and perform experiments at a constant magnetic field, with the superconducting coil in



persistent mode. This eliminates magnetostriction effects on the junction, as the experiment is reset by changing indentation locations and mechanically annealing the contact region at each magnetic field. Furthermore, using the in-situ positioning device described in Ref. <sup>58</sup> we sense many different locations, obtaining an average behavior of hundreds widely different Au and Ag point contacts. Our Au and Ag wires have a purity of 99.99%. From inductively coupled plasma mass spectrometry we find impurities of Si (24 ppm), Fe (17 ppm), Cu (5 ppm), Zn (33 ppm), Ag/Au (100 ppm), Pd (5 ppm), Pt (12 ppm) and Co,Ni < 1 ppm. Such small values are essentially negligible for our results. We took tens of thousands of conductance vs distance curves at each magnetic field and built from these the conductance histograms discussed below. In Fig. 1 we set the zero of the distance at the jump to contact, defined as the point where the conductance increases by more than  $0.3 G_0$  within one pm.

## Modelling the atomic structure of nanocontacts

We generate the Au nanocontact structures discussed in the main text through classical molecular dynamics (CMD) simulations of the pull-push process on a nanowire oriented along the crystallographic direction (001) with a starting narrower middle section. The simulation was performed with the Large-Scale Atomic/Molecular Massively Parallel Simulator (LAMMPS)<sup>62</sup> with an embedded-atom-model (EAM) potential.<sup>63,64</sup> We simulate the pull-push process setting opposite velocities of  $\pm 0.04 \text{ \AA}/\text{ps}$  at each step in the upper and lower layers of the electrode, with steps of 1 ps. The pulling process takes 250 ns and 254 ns for the pushing, to ensure the formation and rupture of the junction in most of the 30 pull-push cycles simulated. The temperature of the system was kept at  $4.2K$  in an NVT canonical ensemble with a Nosé-Hoover thermostat.

We take the central 76 gold atoms from a snapshot of the CMD simulation where a dimer was formed. The atoms in the outer-most layers were re-positioned to form a perfect (001) lattice to prepare the structure for the conductance calculation shown in Fig. 4. The rest, to which an  $O_2$  molecule was randomly added on the surface, were relaxed using the

density functional theory (DFT) implementation in Gaussian16<sup>65</sup> within the unrestricted Local Spin Density Approximation (LSDA). A LANL2DZ basis set<sup>66,67</sup> for the central atoms of gold and oxygen and the minimal basis set CRENS<sup>68</sup> for the outermost layers of gold with the crystalline structure were used.

## Universal binding curve for Au and Ag nanocontacts

To calculate the energy between two atoms bounded to electrodes we build tetrahedral-shaped clusters forming the nanocontact for Au and Ag, as shown in the inset of Fig.S1 (See Supplementary Section I). To obtain the energy  $E$  as a function of the distance  $z$ , we use the density functional theory (DFT) at the GGA level with the PBE<sup>69,70</sup> functional and the D3 version of Grimme’s dispersion with Becke-Johnson damping (GD3BJ)<sup>71</sup> implementation in Gaussian16.<sup>65</sup> We use an all-electron basis-set for Au and Ag, x2c-TZVPall,<sup>72</sup> and incorporate scalar relativistic effects with the use of a Douglas-Kroll-Hess 2nd order scalar relativistic calculation (DKH).<sup>73-76</sup> To perform the calculation, we first optimize the edge length of the regular cluster and then increase the distance between the tips of the two relaxed clusters,  $z$ .

## Transport calculations

We have performed Non-Equilibrium Green’s Functions (NEGF) calculations to obtain the conductance across the junctions obtained as described above. We used our code ANT.Gaussian.<sup>77-81</sup> Here we have used our new implementation that allows us to add a magnetic field in the  $z$ -direction in a self-consistent manner.

## Acknowledgement

We acknowledge discussions with C. Untiedt and N. Agraït. This work was supported by the Spanish Research State Agency (PID2020-114071RB-I00, PDC2021-121086-I00, TED2021-

130546BI00, TED2021-131323B-I00, PID2022-141712NB-C21 and CEX2023001316-M), by the Comunidad de Madrid through program NANOMAGCOST-CM (Program No.S2018/NMT-4321), Generalitat Valenciana through CIDEXG/2022/45 and PROMETEO/2021/017, the EU through grant agreement No 871106 and by the European Research Council PNICTEYES through grant agreements Pnicteyes 679080 and VectorFieldImaging 101069239. This work forms part of the Advanced Materials program and was supported by MCIN with funding from European Union NextGenerationEU (PRTR-C17.I1) and by Generalitat Valenciana (MFA/2022/045). We acknowledge collaborations through EU program Cost CA21144 (superqumap). We acknowledge SEGAINVEX for design and construction of cryogenic equipment and SIDI for support in sample characterization.

## Supplementary Information

### Universal binding curve and other contributions to the energy

The result of the calculation of the binding process for a structure shown in the inset of Fig. S1 is shown by red and blue filled circles in Fig. S1. The shape of the curve is similar for Au and Ag, although there are differences. Whereas the position of the minimum is similar in both elements, the absolute value of the energy at the minimum, or at the equilibrium distance, is much smaller in Au than in Ag.

We can fit the points to the universal binding curve  $E_{UBC}(z) = \alpha(z - z_0)e^{-\beta(z-z_0)}$ .<sup>35-37</sup> We obtain from these parameters the equilibrium bond distance  $d = z_0 + 1/\beta$ , the binding energy  $E_0 = -\alpha/\beta e$  and the breaking force  $F_0 = \alpha/e^2$  (or the slope at the inflection point of  $E_{UBC}(z)$ ) in each element, as shown in Table 1. These values are in agreement with previous work.<sup>30,36,38,82</sup>

Whereas the equilibrium distance  $d$  is quite similar in both elements, the breaking force  $F_0$  and the binding energy  $E_0$  are very different, being much smaller for Ag than for Au.

As discussed in the main text, in the experiment we have to add the contribution to the energy from the leads, which can be modelled by an elastic term  $E_{Elastic} = \frac{k}{2}(D - z)^2$ , with  $k$  being a spring constant and  $D$  the position of the nanoscale leads attached to the contact.<sup>14,38</sup> Adding such an additional quadratic potential, centered at  $D$ , to  $E(z)$  leads to a considerable modification of the energy vs the position (Fig. S2). The minimum in energy is shifted to another position, depending on  $D$ . When  $D$  is large, the elastic potential determines the minimum in energy for the atomic positions, which is located close to  $D$  (magenta curve in Fig. S2). As  $D$  decreases towards zero, the universal binding curve takes over. In between, the curve shows two minima, leading to the usual hysteretic behavior of the formation (decreasing  $D$ ) and rupture (increasing  $D$ ) of a contact. The jump to contact

(decreasing  $D$ ) occurs at a distance  $D_0$  and the conductance is  $G_{a,max}$  exactly just before  $D$  reaches  $D_0$  (blue and black curves in Fig. S2).<sup>38</sup>

Table 1: Values obtained by fitting the universal binding curve.

Element	$d = z_0 + 1/\beta$ (Å)	$E_0 = -\alpha/\beta e$ (eV)	$F_0 = \alpha/e^2$ (Å)
Au	$2.53 \pm 0.02$	$-3.1 \pm 0.2$	$2.24 \pm 0.2$
Ag	$2.6 \pm 0.02$	$-2.33 \pm 0.2$	$1.49 \pm 0.2$

On average over many contacts, the electrodes are similar (similar  $D$ ) in Ag and Au, and also have similar  $k$ . But the value of  $G_{a,max}$  is very different in Ag than in Au already at zero field. In the Fig. 2, left panels, of the main text, we show conductance histograms providing a considerably higher value  $G_{a,max}$  in Ag than in Au. This was found previously in Ref.<sup>30</sup> and is mostly due to the difference in  $E_0$  for both elements. It is important to realize that the behavior of nanocontacts is much more influenced by the elastic term  $\frac{k}{2}(D - z)^2$  in Ag than in Au, because  $|E_0|$  is smaller in Ag than in Au by about 0.8 eV.

We note that  $k$  is related to the elastic constants via  $k \approx \frac{E_Y z_0}{1-\nu^2}$ , with  $E_Y$  the Young modulus and  $\nu$  the Poisson's ratio.<sup>38</sup> The Young modulus is given by the elastic constant  $E_Y = C_{11}$ . There are sizeable differences in  $C_{11}$  and  $C_{12}$  among Ag and Au.<sup>83,84</sup> These lead to differences in the Cauchy pressure ( $C_{11} - C_{44}$ ) and other quantities resulting from combinations of elastic constants. In particular, Poisson's ratio depends on the crystalline direction and the direction of deformation, being generally a combination of all three elastic constants  $C_{11}, C_{12}$  and  $C_{44}$ .<sup>85</sup> These differences lead to a maximal  $\nu$  for Ag and Au of 0.81 and 0.882, respectively.<sup>85</sup> The minimal values of  $\nu$  can however differ by a factor of three, being -0.091 for Ag and -0.029 for Au, when considering modifications due to stretching along the direction [110]. Notice that the Poisson's ratio is negative, as Au and Ag are both auxetic (laterally expanding when stretched along [110]) due to many body contributions to the binding energy.<sup>85</sup> Nevertheless, such changes in  $\nu$  have little influence on changes in  $k$  related to the element. Furthermore the spring constant  $k$  strongly varies with the atomic arrangements close to the contact. Crystalline orientation, defects and angle of the

contact with a high symmetry direction, provide numerous situations with different  $k$  and thus determine the spread of values of  $G_a$ .<sup>14,37,38,38</sup> Although there are slight differences in the spread of  $G_a$ , depending on the experimental run, as discussed in Ref. ,<sup>30</sup> the difference observed in  $G_{a,max}$  is well above the spread and shows directly how different the universal binding curves are for both elements, Au being stiffer than Ag.

Therefore, the addition of a magnetic term  $E_{Magnetic}$  to the energy has a much stronger influence in  $G_{a,max}$  in Ag than in Au.

To estimate the magnetic contribution, we can consider the susceptibility of bulk Au (the largest contribution, which is diamagnetic is of  $\chi_{Au} = -3.4 \times 10^{-5}$ , a similar value is found in Ag<sup>41,86</sup>). If we then take into account the shape anisotropy of a cylinder and obtain  $\chi_{anis} = \chi_{||} - \chi_{\perp} \approx 10^{-10}$ .<sup>87</sup> We estimate the magnetic field induced  $E_{Magnetic} \approx \chi_{anis} V \frac{B^2}{\mu_0} \sin(\theta)$ , as in the main text. Assuming that the magnetically active volume is approximated by a sphere with radius of 100 nm, and that  $\theta$  is of a few tens of degree we obtain  $E_{mag} \approx 6 \times 10^{-7}$  eV. This is far below any relevant value in the expression for  $E(z)$ . Thus, the magnetism of Au or Ag itself does not produce any sizeable effect on the nanocontact.

The formation of nanometric sized necks around the single atom point contact through repeated indentation leads to anisotropic wire like structures around the contact, of a few tens of nm length.<sup>88</sup> The macroscopic currents circulating in these leads can provide, as shown in the main text, much larger values of  $E_{mag}$ .

## Sticking and magnetism of O<sub>2</sub> at surfaces

Studies of gold-oxygen chains have shown that a hybrid orbital structure between Au and O<sub>2</sub> provides strongest bonding.<sup>47</sup> Whereas chemisorbed O<sub>2</sub> loses its magnetic moment (having either 1  $\mu_B$  or none), physisorbed O<sub>2</sub> maintains a magnetic moment of 2  $\mu_B$ .<sup>46,89</sup> In physisorbed O<sub>2</sub>, the spin up and spin down states of the O<sub>2</sub> orbitals that are closest to the Fermi level are spin split  $\pi_p$  orbitals, with a gap between spin polarized bands of more than

1 eV.<sup>90</sup> In the gold-oxygen chains, mixed orbitals derived mostly from Au s electrons with a small contribution from O p electrons form, providing bands with a small spin splitted gap.<sup>47</sup> There is however no clear indication for a strong magnetic field effect on the conduction.

For Au, a magnetic moment of  $1.3 \times 10^{-4} \mu_B/\text{atom}$  in an applied magnetic field of 10 T has been observed.<sup>86</sup> Furthermore, the paramagnetic susceptibility for the 5d orbit is of  $8.9 \times 10^{-6}$  and is characterized by a strong orbital contribution.<sup>86,91</sup> These small values eliminate any significant intrinsic effect of the magnetic field on the conduction through an Au single atom point contact.

The force required to move metal atoms on a surface depends strongly on the bonding to the substrate and can be of the order of pN even for well bonded metals (e.g. 17 pN for Co on Cu).<sup>92</sup> The push-pull process during the conductance vs distance curves and the magnetic field is thus very effective to add considerable mobility to O<sub>2</sub> molecules. Close to the contact area, O<sub>2</sub> take advantage of the reduction of the Au coordination and can stick.

## Magnetic anisotropy energy

The magnetic anisotropy energy (MAE) was estimated on a toy model contact of two Au pyramids of crystalline (001) Au with layers of 1-4-9 Au atoms. This model was completed with an O<sub>2</sub> molecule aligned in the z direction, as shown in Fig.S3. ANT.Gaussian has a newly build-in module to add self-consistent Spin-Orbit Coupling (SOC). We use this module and a modified basis set Au\_pob\_TZPV\_rev2<sup>93,94</sup> to add SOC to the central gold atoms of the toy model. We performed a single-point energy calculation with accuracy up to  $3 \times 10^{-8}$  eV with the spin fixed to the directions x,y,z with and without SOC.

For model V (Fig.S3), the difference in energy between the spin directions without SOC is approx.  $3 \times 10^{-7}$  eV, which corresponds to the numerical accuracy of the calculations. It is negligible in comparison with the difference between the z-direction, which has the lowest energy, and the x/y-direction with SOC,  $6.5 \times 10^{-4}$  eV. In model H (Fig.S3), the difference

without SOC is of  $6 \times 10^{-6}$  eV, and with SOC the lowest energy is obtained in the x-direction, with differences of  $8 \times 10^{-5}$  eV with the y/z-directions. This result infers the existence of an easy and hard axis in this system, which is induced on the molecule by the strong SOC of Au. Moreover, we can say that the MAE induced by Au depends on the binding geometry of the O<sub>2</sub>.

## References

- (1) Agraït, N.; Yeyati, A. L.; van Ruitenbeek, J. M. Quantum properties of atomic-sized conductors. *Physics Reports* **2003**, *377*, 81–279.
- (2) Requist, R.; Baruselli, P. P.; Smogunov, A.; Fabrizio, M.; Modesti, S.; Tosatti, E. Metallic, magnetic and molecular nanocontacts. *Nature Nanotechnology* **2016**, *11*, 499–508.
- (3) Heinrich, A. J.; Oliver, W. D.; Vandersypen, L. M. K.; Ardavan, A.; Sessoli, R.; Loss, D.; Jayich, A. B.; Fernández-Rossier, J.; Laucht, A.; Morello, A. Quantum-coherent nanoscience. *Nature Nanotechnology* **2021**, *16*, 1318–1329.
- (4) Krans, J. M.; van Ruitenbeek, J. M.; Fisun, V. V.; Yanson, I. K.; de Jongh, L. J. The signature of conductance quantization in metallic point contacts. *Nature* **1995**, *375*, 767–769.
- (5) Ohnishi, H.; Kondo, Y.; Takayanagi, K. Quantized conductance through individual rows of suspended gold atoms. *Nature* **1998**, *395*, 780–783.
- (6) Yanson, A. I.; Bollinger, G. R.; van den Brom, H. E.; Agraït, N.; van Ruitenbeek, J. M. Formation and manipulation of a metallic wire of single gold atoms. *Nature* **1998**, *395*, 783–785.
- (7) Fernández, M. A.; Sabater, C.; Dednam, W.; Palacios, J. J.; Calvo, M. R.; Untiedt, C.;



- Caturla, M. J. Dynamic bonding of metallic nanocontacts: Insights from experiments and atomistic simulations. *Phys. Rev. B* **2016**, *93*, 085437.
- (8) Landauer, R. Spatial Variation of Currents and Fields Due to Localized Scatterers in Metallic Conduction. *IBM Journal of Research and Development* **1957**, *1*, 223–231.
- (9) Nazarov, Y.; Blanter, Y. *Quantum transport-Introduction to nanoscience*; Cambridge University Press, 2009.
- (10) Scheer, E.; Agraït, N.; Cuevas, J. C.; Yeyati, A. L.; Ludoph, B.; Martín-Rodero, A.; Bollinger, G. R.; van Ruitenbeek, J. M.; Urbina, C. The signature of chemical valence in the electrical conduction through a single-atom contact. *Nature* **1998**, *394*, 154–157.
- (11) Agraït, N.; Rodrigo, J. G.; Vieira, S. Conductance steps and quantization in atomic-size contacts. *Phys. Rev. B* **1993**, *47*, 12345–12348.
- (12) Untiedt, C.; Yanson, A. I.; Grande, R.; Rubio-Bollinger, G.; Agraït, N.; Vieira, S.; van Ruitenbeek, J. Calibration of the length of a chain of single gold atoms. *Phys. Rev. B* **2002**, *66*, 085418.
- (13) Cuevas, J. C.; Levy Yeyati, A.; Martín-Rodero, A.; Rubio Bollinger, G.; Untiedt, C.; Agraït, N. Evolution of Conducting Channels in Metallic Atomic Contacts under Elastic Deformation. *Phys. Rev. Lett.* **1998**, *81*, 2990–2993.
- (14) Rubio-Bollinger, G.; Bahn, S. R.; Agraït, N.; Jacobsen, K. W.; Vieira, S. Mechanical Properties and Formation Mechanisms of a Wire of Single Gold Atoms. *Phys. Rev. Lett.* **2001**, *87*, 026101.
- (15) Smit, R. H. M.; Untiedt, C.; Yanson, A. I.; van Ruitenbeek, J. M. Common Origin for Surface Reconstruction and the Formation of Chains of Metal Atoms. *Phys. Rev. Lett.* **2001**, *87*, 266102.

- (16) Rodrigues, V.; Bettini, J.; Silva, P. C.; Ugarte, D. Evidence for Spontaneous Spin-Polarized Transport in Magnetic Nanowires. *Phys. Rev. Lett.* **2003**, *91*, 096801.
- (17) Untiedt, C.; Dekker, D. M. T.; Djukic, D.; van Ruitenbeek, J. M. Absence of magnetically induced fractional quantization in atomic contacts. *Phys. Rev. B* **2004**, *69*, 081401.
- (18) Fernández-Rossier, J.; Jacob, D.; Untiedt, C.; Palacios, J. J. Transport in magnetically ordered Pt nanocontacts. *Phys. Rev. B* **2005**, *72*, 224418.
- (19) Strigl, F.; Espy, C.; Bückle, M.; Scheer, E.; Pietsch, T. Emerging magnetic order in platinum atomic contacts and chains. *Nature Communications* **2015**, *6*, 6172.
- (20) Kinikar, A.; Phanindra Sai, T.; Bhattacharyya, S.; Agarwala, A.; Biswas, T.; Sarker, S. K.; Krishnamurthy, H. R.; Jain, M.; Shenoy, V. B.; Ghosh, A. Quantized edge modes in atomic-scale point contacts in graphene. *Nature Nanotechnology* **2017**, *12*, 564–568.
- (21) Kawamura, M.; Ono, K.; Stano, P.; Kono, K.; Aono, T. Electronic Magnetization of a Quantum Point Contact Measured by Nuclear Magnetic Resonance. *Phys. Rev. Lett.* **2015**, *115*, 036601.
- (22) Brun, B.; Martins, F.; Faniel, S.; Hackens, B.; Bachelier, G.; Cavanna, A.; Ulysse, C.; Ouerghi, A.; Gennser, U.; Maily, D.; Huant, S.; Bayot, V.; Sanquer, M.; Sellier, H. Wigner and Kondo physics in quantum point contacts revealed by scanning gate microscopy. *Nature Communications* **2014**, *5*, 4290.
- (23) Bagrets, A.; Papanikolaou, N.; Mertig, I. Magnetoresistance of atomic-sized contacts: An ab initio study. *Phys. Rev. B* **2004**, *70*, 064410.
- (24) Jacob, D.; Fernández-Rossier, J.; Palacios, J. J. Magnetic and orbital blocking in Ni nanocontacts. *Phys. Rev. B* **2005**, *71*, 220403.

- (25) Suderow, H.; Crespo, M.; Vieira, S.; Vila, M.; García-Hernández, M.; de Andrés, A.; Prieto, C.; Ocal, C.; Martínez, J.; Mukovskii, Y. Observation of a spin-polarized current through single atom quantum point contacts. *Physica E: Low-dimensional Systems and Nanostructures* **2003**, *18*, 264–265, 23rd International Conference on Low Temperature Physics (LT23).
- (26) Doudin, B.; Viret, M. Ballistic magnetoresistance? *Journal of Physics: Condensed Matter* **2008**, *20*, 083201.
- (27) Calvo, M. R.; Fernández-Rossier, J.; Palacios, J. J.; Jacob, D.; Natelson, D.; Untiedt, C. The Kondo effect in ferromagnetic atomic contacts. *Nature* **2009**, *458*, 1150–1153.
- (28) Vardimon, R.; Klionsky, M.; Tal, O. Experimental determination of conduction channels in atomic-scale conductors based on shot noise measurements. *Phys. Rev. B* **2013**, *88*, 161404.
- (29) Cuevas, J. C.; Yeyati, A. L.; Martín-Rodero, A. Microscopic Origin of Conducting Channels in Metallic Atomic-Size Contacts. *Phys. Rev. Lett.* **1998**, *80*, 1066–1069.
- (30) Calvo, M. R.; Sabater, C.; Dednam, W.; Lombardi, E. B.; Caturla, M. J.; Untiedt, C. Influence of Relativistic Effects on the Contact Formation of Transition Metals. *Phys. Rev. Lett.* **2018**, *120*, 076802.
- (31) Sabater, C.; Caturla, M. J.; Palacios, J. J.; Untiedt, C. Understanding the structure of the first atomic contact in gold. *Nanoscale Research Letters* **2013**, *8*, 257.
- (32) Sabater, C.; Dednam, W.; Calvo, M. R.; Fernández, M. A.; Untiedt, C.; Caturla, M. J. Role of first-neighbor geometry in the electronic and mechanical properties of atomic contacts. *Phys. Rev. B* **2018**, *97*, 075418.
- (33) Dednam, W.; Tewari, S.; Lombardi, E. B.; Palacios, J. J.; van Ruitenbeek, J. M.;

- Sabater, C. Dynamic bonding influenced by the proximity of adatoms to one atom high step edges. *Phys. Rev. B* **2022**, *106*, 125418.
- (34) Dednam, W.; Sabater, C.; Fernandez, M. A.; Untiedt, C.; Palacios, J. J.; Caturla, M. J. Modeling contact formation between atomic-sized gold tips via molecular dynamics. *Journal of Physics: Conference Series* **2015**, *574*, 012045.
- (35) Rose, J. H.; Ferrante, J.; Smith, J. R. Universal Binding Energy Curves for Metals and Bimetallic Interfaces. *Phys. Rev. Lett.* **1981**, *47*, 675–678.
- (36) Bahn, S. R.; Jacobsen, K. W. Chain Formation of Metal Atoms. *Phys. Rev. Lett.* **2001**, *87*, 266101.
- (37) Rodrigues, V.; Fuhrer, T.; Ugarte, D. Signature of Atomic Structure in the Quantum Conductance of Gold Nanowires. *Phys. Rev. Lett.* **2000**, *85*, 4124–4127.
- (38) Trouwborst, M. L.; Huisman, E. H.; Bakker, F. L.; van der Molen, S. J.; van Wees, B. J. Single Atom Adhesion in Optimized Gold Nanojunctions. *Phys. Rev. Lett.* **2008**, *100*, 175502.
- (39) Sabater, C.; Untiedt, C.; Palacios, J. J.; Caturla, M. J. Mechanical Annealing of Metallic Electrodes at the Atomic Scale. *Phys. Rev. Lett.* **2012**, *108*, 205502.
- (40) Ostapiak, O. Z.; Perz, J. M. Stress dependence of the Fermi surface of gold. *Phys. Rev. B* **1993**, *48*, 17001–17005.
- (41) van Rhee, P. G.; Zijlstra, P.; Verhagen, T. G. A.; Aarts, J.; Katsnelson, M. I.; Maan, J. C.; Orrit, M.; Christianen, P. C. M. Giant Magnetic Susceptibility of Gold Nanorods Detected by Magnetic Alignment. *Phys. Rev. Lett.* **2013**, *111*, 127202.
- (42) Garitaonandia, J. S.; Insausti, M.; Goikolea, E.; Suzuki, M.; Cashion, J. D.; Kawamura, N.; Ohsawa, H.; Gil de Muro, I.; Suzuki, K.; Plazaola, F.; Rojo, T. Chemically

- Induced Permanent Magnetism in Au, Ag, and Cu Nanoparticles Localization of the Magnetism by Element Selective Techniques. *Nano Letters* **2008**, *8*, 661–667.
- (43) Hernando, A.; Ayuela, A.; Crespo, P.; Echenique, P. M. Giant diamagnetism of gold nanorods. *New Journal of Physics* **2014**, *16*, 073043.
- (44) Thijssen, W. H. A.; Marjenburgh, D.; Bremmer, R. H.; van Ruitenbeek, J. M. Oxygen-Enhanced Atomic Chain Formation. *Phys. Rev. Lett.* **2006**, *96*, 026806.
- (45) Thijssen, W. H. A.; Strange, M.; aan de Brugh, J. M. J.; van Ruitenbeek, J. M. Formation and properties of metal–oxygen atomic chains. *New Journal of Physics* **2008**, *10*, 033005.
- (46) Montemore, M. M.; van Spronsen, M. A.; Madix, R. J.; Friend, C. M. O<sub>2</sub> Activation by Metal Surfaces: Implications for Bonding and Reactivity on Heterogeneous Catalysts. *Chemical Reviews* **2018**, *118*, 2816–2862.
- (47) Bahn, S. R.; López, N.; Nørskov, J. K.; Jacobsen, K. W. Adsorption-induced restructuring of gold nanochains. *Phys. Rev. B* **2002**, *66*, 081405.
- (48) Woodham, A. P.; Meijer, G.; Fielicke, A. Charge Separation Promoted Activation of Molecular Oxygen by Neutral Gold Clusters. *Journal of the American Chemical Society* **2013**, *135*, 1727–1730.
- (49) Kurahashi, M. Oxygen adsorption on surfaces studied by a spin- and alignment-controlled O<sub>2</sub> beam. *Progress in Surface Science* **2016**, *91*, 29–55.
- (50) Kurahashi, M. Chemisorption of aligned O<sub>2</sub> on Ag(110). *The Journal of Chemical Physics* **2019**, *151*, 084702.
- (51) Luntz, A.; Williams, M.; Bethune, D. The sticking of O<sub>2</sub> on a Pt(111) surface. *The Journal of Chemical Physics* **1988**, *89*, 4381 – 4395.

- (52) Zhao, Z.; Wang, Y.; Yang, X.; Quan, J.; Krüger, B. C.; Stoicescu, P.; Nieman, R.; Auerbach, D. J.; Wodtke, A. M.; Guo, H.; Park, G. B. Spin-dependent reactivity and spin-flipping dynamics in oxygen atom scattering from graphite. *Nature Chemistry* **2023**, *15*, 1006–1011.
- (53) Brune, H.; Wintterlin, J.; Behm, R. J.; Ertl, G. Surface migration of “hot” adatoms in the course of dissociative chemisorption of oxygen on Al(111). *Phys. Rev. Lett.* **1992**, *68*, 624–626.
- (54) Behler, J.; Delley, B.; Lorenz, S.; Reuter, K.; Scheffler, M. Dissociation of O<sub>2</sub> at Al(111): The Role of Spin Selection Rules. *Phys. Rev. Lett.* **2005**, *94*, 036104.
- (55) Österlund, L.; Zoric-acute, I.; Kasemo, B. Dissociative sticking of O<sub>2</sub> on Al(111). *Phys. Rev. B* **1997**, *55*, 15452–15455.
- (56) Fernández-Lomana, M.; Wu, B.; Martín-Vega, F.; Sánchez-Barquilla, R.; Álvarez Montoya, R.; Castilla, J. M.; Navarrete, J.; Marijuan, J. R.; Herrera, E.; Suderow, H.; Guillamón, I. Millikelvin scanning tunneling microscope at 20/22 T with a graphite enabled stick–slip approach and an energy resolution below 8  $\mu\text{eV}$ : Application to conductance quantization at 20 T in single atom point contacts of Al and Au and to the charge density wave of 2H–NbSe<sub>2</sub>. *Review of Scientific Instruments* **2021**, *92*, 093701.
- (57) Martín-Vega, F. et al. Simplified feedback control system for scanning tunneling microscopy. *Review of Scientific Instruments* **2021**, *92*, 103705.
- (58) Suderow, H.; Guillamón, I.; Vieira, S. Compact very low temperature scanning tunneling microscope with mechanically driven horizontal linear positioning stage. *Review of Scientific Instruments* **2011**, *82*, 033711.
- (59) Agraït, N.; Untiedt, C.; Rubio-Bollinger, G.; Vieira, S. Onset of Energy Dissipation in Ballistic Atomic Wires. *Phys. Rev. Lett.* **2002**, *88*, 216803.

- (60) Untiedt, C.; Rubio Bollinger, G.; Vieira, S.; Agraït, N. Quantum interference in atomic-sized point contacts. *Phys. Rev. B* **2000**, *62*, 9962–9965.
- (61) Rubio-Bollinger, G.; Joyez, P.; Agraït, N. Metallic Adhesion in Atomic-Size Junctions. *Phys. Rev. Lett.* **2004**, *93*, 116803.
- (62) Thompson, A. P.; Aktulga, H. M.; Berger, R.; Bolintineanu, D. S.; Brown, W. M.; Crozier, P. S.; in 't Veld, P. J.; Kohlmeyer, A.; Moore, S. G.; Nguyen, T. D.; Shan, R.; Stevens, M. J.; Tranchida, J.; Trott, C.; Plimpton, S. J. LAMMPS - a flexible simulation tool for particle-based materials modeling at the atomic, meso, and continuum scales. *Computer physics communications* **2022**, *271*, 108171.
- (63) Zhou, X. W.; Johnson, R. A.; Wadley, H. N. G. Misfit-energy-increasing dislocations in vapor-deposited CoFe/NiFe multilayers. *Physical review. B, Condensed matter and materials physics* **2004**, *69*.
- (64) Zhou, X.; Johnson, R.; Wadley, H. *EAM potential (LAMMPS cubic hermite tabulation) for Au developed by Zhou, Johnson and Wadley (2004) v005*; OpenKIM, 2018.
- (65) Frisch, M. J. et al. Gaussian~16 Revision C.01. 2016; Gaussian Inc. Wallingford CT.
- (66) *Methods of electronic structure theory*; Springer US: Boston, MA, 1977.
- (67) Hay, P. J.; Wadt, W. R. Ab initio effective core potentials for molecular calculations. Potentials for K to Au including the outermost core orbitals. *The Journal of chemical physics* **1985**, *82*, 299–310.
- (68) Ross, R. B.; Powers, J. M.; Atashroo, T.; Ermler, W. C.; LaJohn, L. A.; Christiansen, P. A. Erratum: Ab initio relativistic effective potentials with spin-orbit operators. IV. Cs through Rn [J. Chem. Phys. 93, 6654 (1990)]. *The Journal of chemical physics* **1994**, *101*, 10198–10198.

- (69) Perdew, J. P.; Burke, K.; Ernzerhof, M. Generalized gradient approximation made simple. *Physical review letters* **1996**, *77*, 3865–3868.
- (70) Perdew, J. P.; Burke, K.; Ernzerhof, M. Generalized gradient approximation made simple [phys. Rev. Lett. 77, 3865 (1996)]. *Physical review letters* **1997**, *78*, 1396–1396.
- (71) Grimme, S.; Ehrlich, S.; Goerigk, L. Effect of the damping function in dispersion corrected density functional theory. *Journal of computational chemistry* **2011**, *32*, 1456–1465.
- (72) Pollak, P.; Weigend, F. Segmented contracted error-consistent basis sets of double- and triple- $\zeta$  valence quality for one- and two-component relativistic all-electron calculations. *Journal of chemical theory and computation* **2017**, *13*, 3696–3705.
- (73) Douglas, M.; Kroll, N. M. Quantum electrodynamical corrections to the fine structure of helium. *Annals of physics* **1974**, *82*, 89–155.
- (74) Hess, B. A. Applicability of the no-pair equation with free-particle projection operators to atomic and molecular structure calculations. *Physical review A: General physics* **1985**, *32*, 756–763.
- (75) Hess, B. A. Relativistic electronic-structure calculations employing a two-component no-pair formalism with external-field projection operators. *Physical review A: General physics* **1986**, *33*, 3742–3748.
- (76) Jansen, G.; Hess, B. A. Revision of the Douglas-Kroll transformation. *Physical review A: General physics* **1989**, *39*, 6016–6017.
- (77) Jacob, D.; Palacios, J. J. Critical comparison of electrode models in density functional theory based quantum transport calculations. *The Journal of chemical physics* **2011**, *134*, 044118.



- (78) Palacios, J. J.; Pérez-Jiménez, A. J.; Louis, E.; SanFabián, E.; Vergés, J. A. First-principles approach to electrical transport in atomic-scale nanostructures. *Physical review. B, Condensed matter* **2002**, *66*.
- (79) Palacios, J. J.; Pérez-Jiménez, A. J.; Louis, E.; SanFabián, E.; Vergés, J. A.; García, Y. *Computational Chemistry: Reviews of Current Trends*; WORLD SCIENTIFIC, 2005; p 1–46.
- (80) Jacob, D.; Fernández-Rossier, J.; Palacios, J. J. Magnetic and orbital blocking in Ni nanocontacts. *Physical review. B, Condensed matter and materials physics* **2005**, *71*.
- (81) Dednam, W.; Zotti, L. A.; Palacios, J. J. Computer code ANT.Gaussian, with SOC corrections. Available from <https://github.com/juanjosepalacios/ANT.Gaussian>, Date of access: 21-Jun-2024.
- (82) Hammer, B.; Nørskov, J. *Impact of Surface Science on Catalysis*; Advances in Catalysis; Academic Press, 2000; Vol. 45; pp 71–129.
- (83) Neighbours, J. R.; Alers, G. A. Elastic Constants of Silver and Gold. *Phys. Rev.* **1958**, *111*, 707–712.
- (84) Lide, D. R. CRC Handbook of Chemistry and Physics. **2005**,
- (85) Baughman, R. H.; Shacklette, J. M.; Zakhidov, A. A.; Stafström, S. Negative Poisson's ratios as a common feature of cubic metals. *Nature* **1998**, *392*, 362–365.
- (86) Suzuki, M.; Kawamura, N.; Miyagawa, H.; Garitaonandia, J. S.; Yamamoto, Y.; Hori, H. Measurement of a Pauli and Orbital Paramagnetic State in Bulk Gold Using X-Ray Magnetic Circular Dichroism Spectroscopy. *Phys. Rev. Lett.* **2012**, *108*, 047201.
- (87) Prozorov, R.; Kogan, V. G. Effective Demagnetizing Factors of Diamagnetic Samples of Various Shapes. *Phys. Rev. Appl.* **2018**, *10*, 014030.

- (88) Untiedt, C.; Rubio, G.; Vieira, S.; Agraït, N. Fabrication and characterization of metallic nanowires. *Phys. Rev. B* **1997**, *56*, 2154–2160.
- (89) Alducin, M.; Sánchez-Portal, D.; Arnau, A.; Lorente, N. Mixed-Valency Signature in Vibrational Inelastic Electron Tunneling Spectroscopy. *Phys. Rev. Lett.* **2010**, *104*, 136101.
- (90) Mkhonto, P. P.; Chauke, H. R.; Ngoepe, P. E. Ab initio Studies of O<sub>2</sub> Adsorption on (110) Nickel-Rich Pentlandite (Fe<sub>4</sub>Ni<sub>5</sub>S<sub>8</sub>) Mineral Surface. *Minerals* **2015**, *5*, 665–678.
- (91) Trudel, S. Unexpected magnetism in gold nanostructures: making gold even more attractive. *Gold Bulletin* **2011**, *44*, 3–13.
- (92) Ternes, M.; Lutz, C. P.; Hirjibehedin, C. F.; Giessibl, F. J.; Heinrich, A. J. The Force Needed to Move an Atom on a Surface. *Science* **2008**, *319*, 1066–1069.
- (93) Laun, J.; Bredow, T. BSSE-corrected consistent Gaussian basis sets of triple-zeta valence with polarization quality of the fifth period for solid-state calculations. *Journal of computational chemistry* **2022**, *43*, 839–846.
- (94) Figgen, D.; Rauhut, G.; Dolg, M.; Stoll, H. Energy-consistent pseudopotentials for group 11 and 12 atoms: adjustment to multi-configuration Dirac–Hartree–Fock data. *Chemical physics* **2005**, *311*, 227–244.

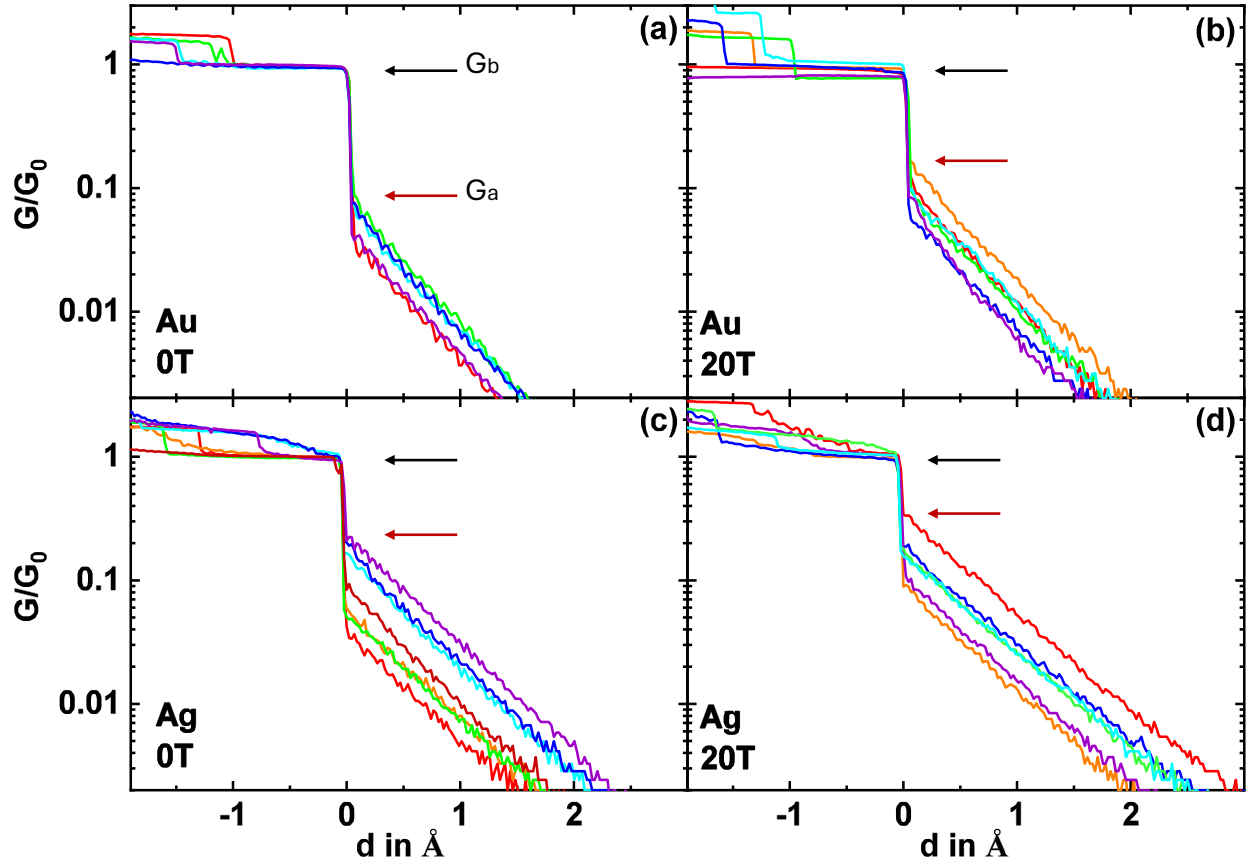


Figure 1: (a-d) We show as colored lines measurements of the conductance  $G$  vs distance  $d$  in single atom point contacts of Ag and Au. We set  $d = 0$  at the contact formation. For  $d > 0$ , we observe the exponential dependence characteristic of the tunneling regime. Curves are taken by moving the z-position of the tip from the tunneling into the contact regime (from the right to the left in the figure). The red arrows mark the conductance just before the formation of the contact,  $G_a$ . The black arrows mark the conductance of the single atom contact,  $G_b$ . Data are taken at zero magnetic field (a,c) and under a magnetic field of 20 T (b,d). The conductance  $G$  is normalized to the quantum of conductance  $G_0 = \frac{2e^2}{h}$ .

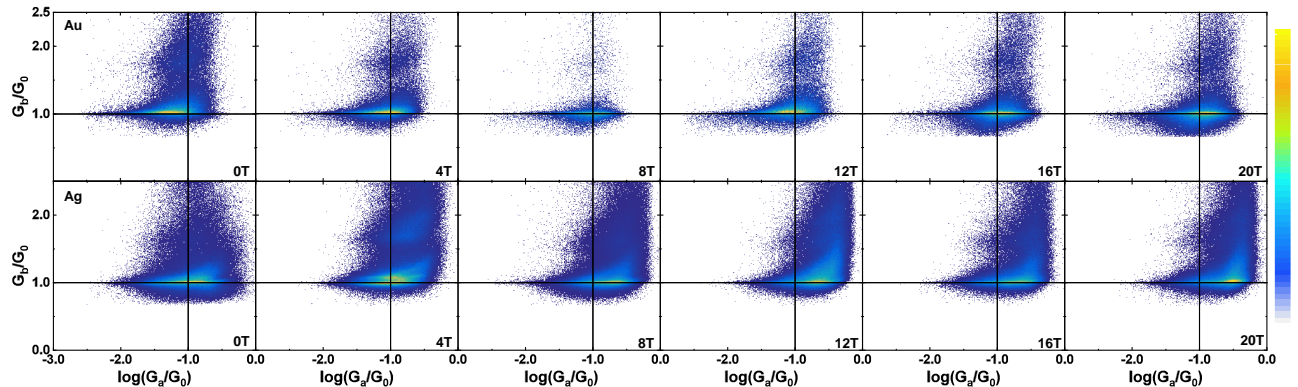


Figure 2: We show in a color scale histograms of the single atom point contact conductance  $G_b$  (y axis) and of the conductance just before the contact formation,  $G_a$  (x axis). Conductance values are normalized to the quantum of conductance  $G_0$ . Frequent occurrences are shown in yellow, and none in white, following the bar on the right. Data are for Au (top row) and Ag (bottom row). The magnetic field is indicated in each panel. Black lines are a guide to the eye. We see that the conductance of the single atom point contacts is very well defined and often located at  $G_b = G_0$ . The conductance just before the jump to contact  $G_a$  is slightly larger in Ag than in Au, as found previously at zero magnetic field in Ref. <sup>30</sup> and increases with the magnetic field in Ag. We also see that, while Ag contacts do not occur for  $G_b < G_0$ , there is an increasing number of Au contacts with  $G_b < G_0$  under magnetic fields.

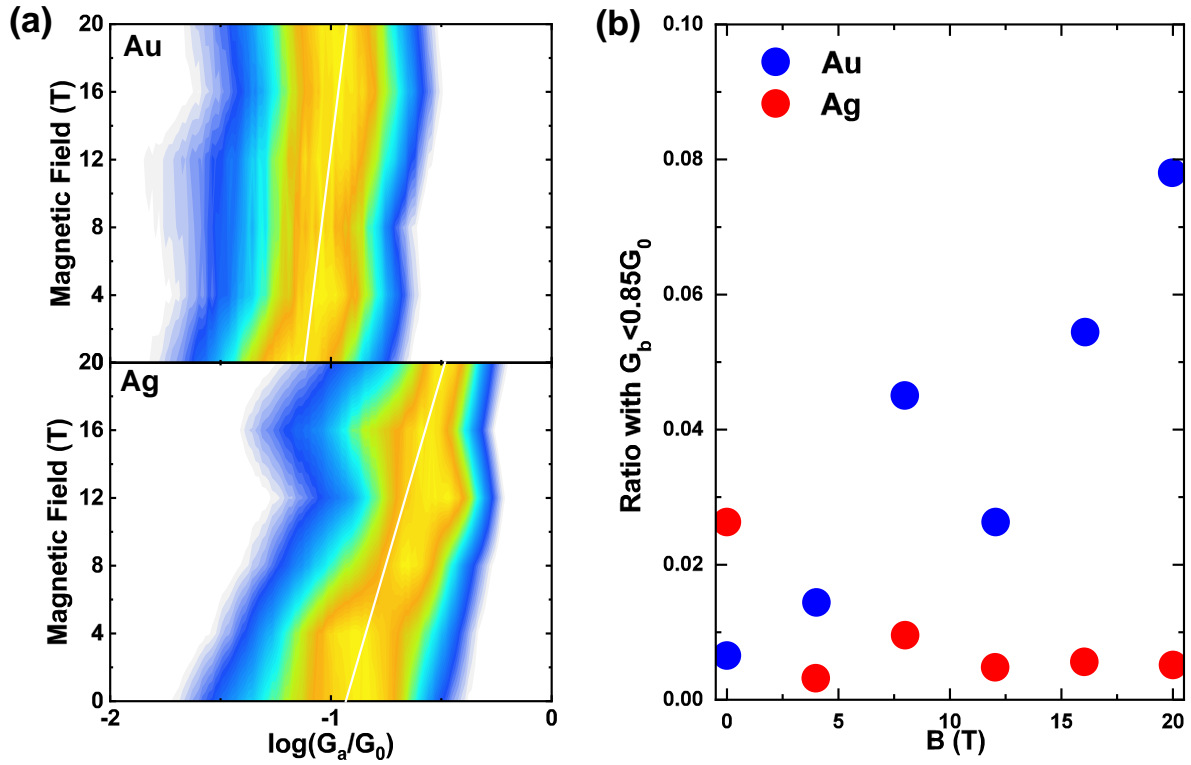


Figure 3: (a) We show as a color scale histograms of the conductance before jump to contact,  $G_a$ , obtained for  $G_b = 1$ , as a function of the magnetic field, for Au (top panel) and for Ag (bottom panel). White lines are guides to the eye. (b) Ratio of single atom point contacts with  $G_b < 0.85G_0$  as a function of the magnetic field (blue points for Au and red points for Ag).

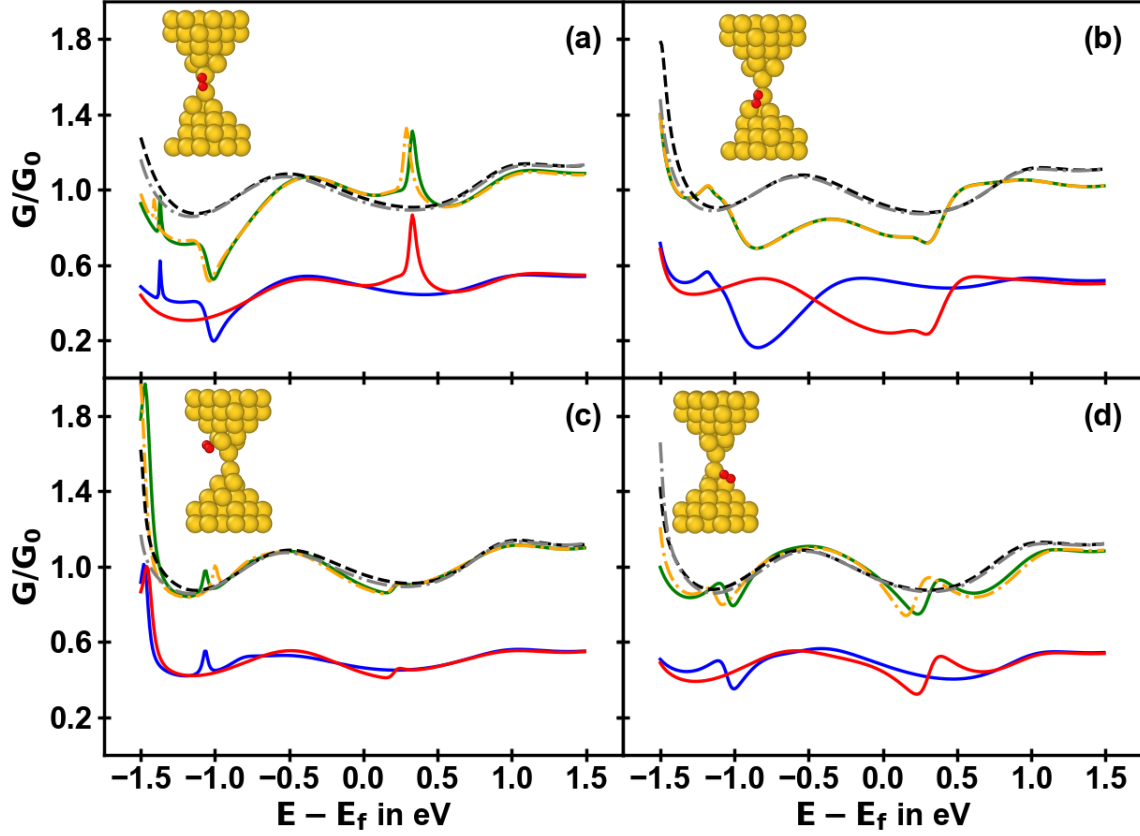


Figure 4: (a-d) We show as colored lines the conductance as a function of the energy (minus the Fermi energy) for single atom point contacts of Au calculated as described in the text. Dashed black line is for the conductance of a single atom point contact of Au at zero magnetic field and the grey dashed line is for the 20 T case. Green (zero field) and yellow (20 T) dashed lines are for single atom point contacts of Au with an  $O_2$  molecule attached to the contact, located at the position shown in the upper left insets in all panels (a-d). Red and blue lines are the conductance for spin up and spin down electrons, respectively.

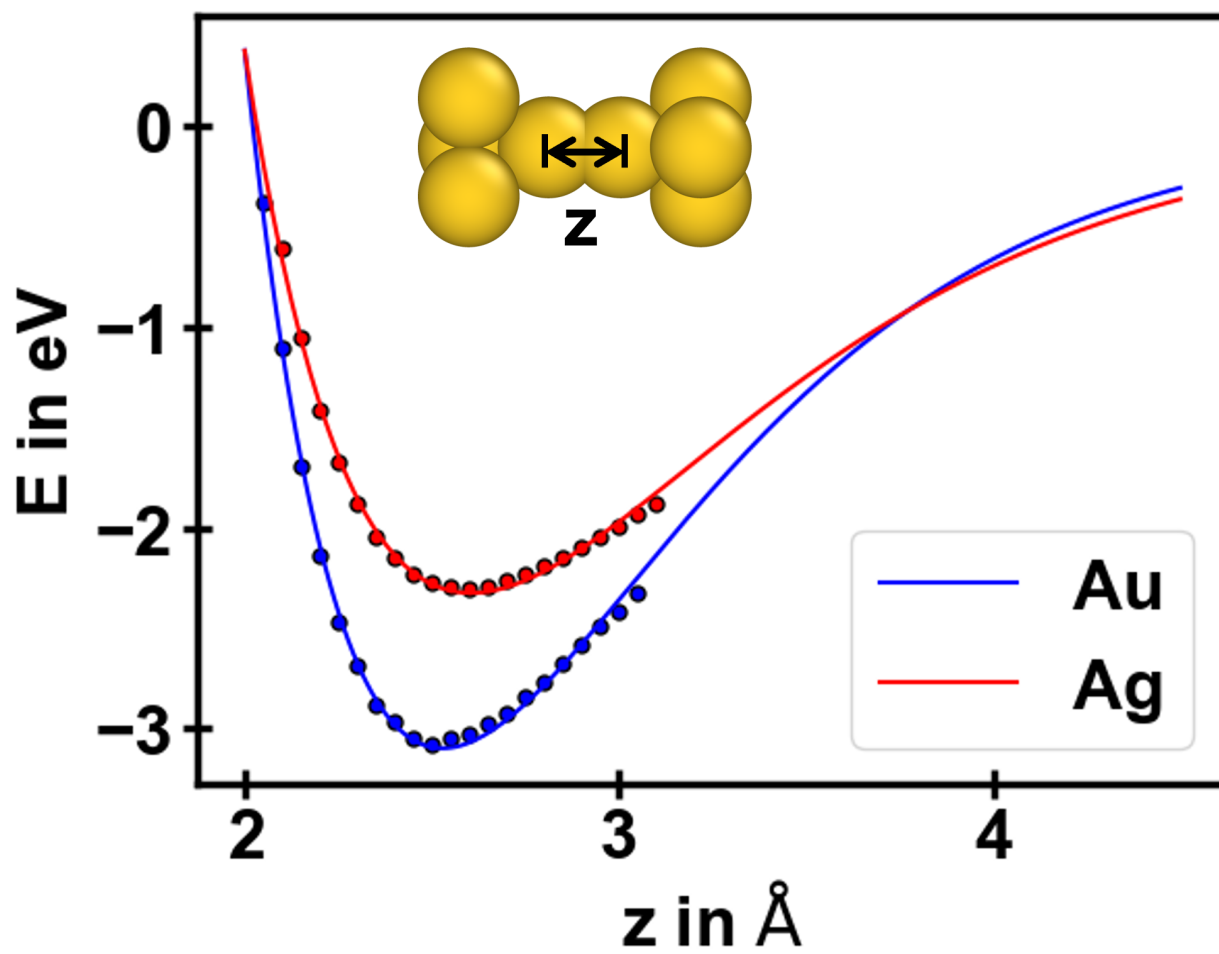


Figure S1: Binding energy with vs distance between the centers of the atoms at the tip, as shown in the inset. Calculated points of data are represented with a dot, whereas the fit to the binding curve is plotted as a solid line.

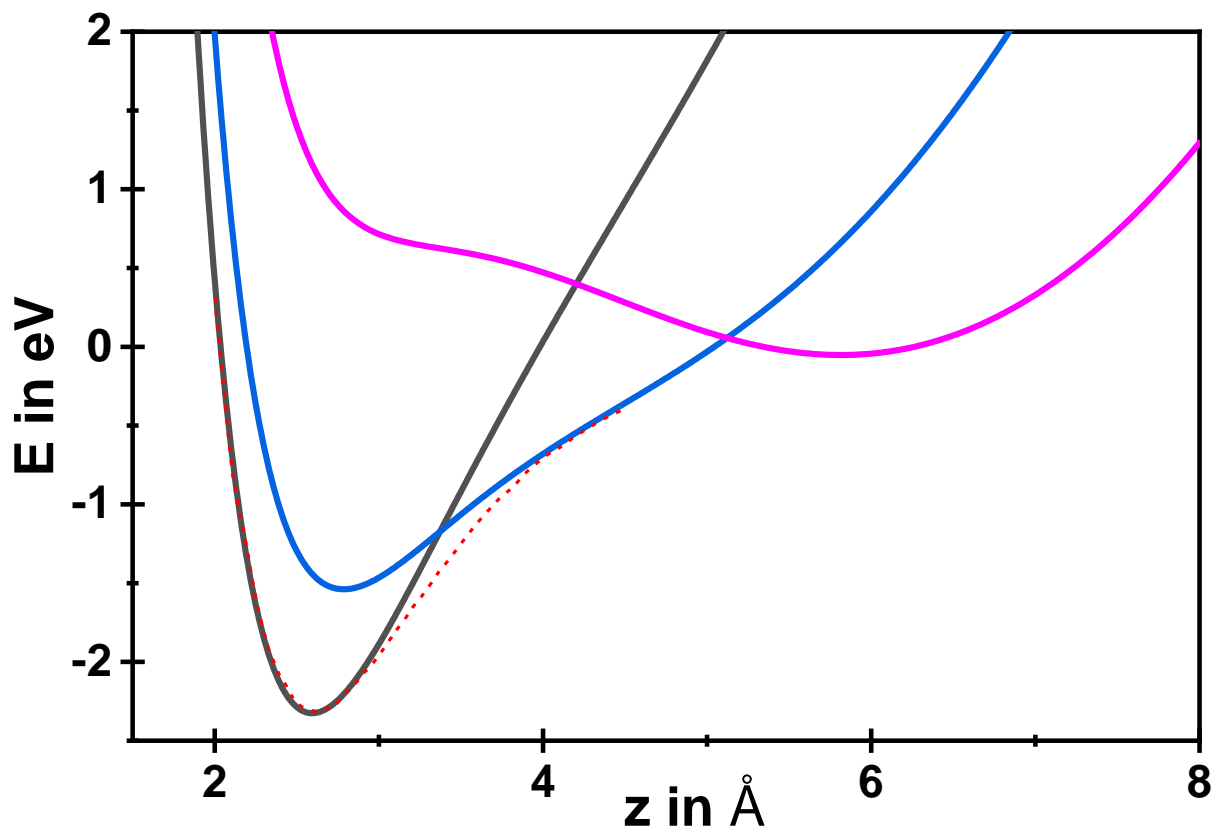


Figure S2: Energy  $E_{UBC} + E_{Elastic}$  vs distance for different values of the distance between electrodes  $D$  and contacts between Ag electrodes. Curves for tip and sample far away is shown in magenta, close to contact in blue and in good contact in black. The universal binding curve for Ag is shown by dashed red line.



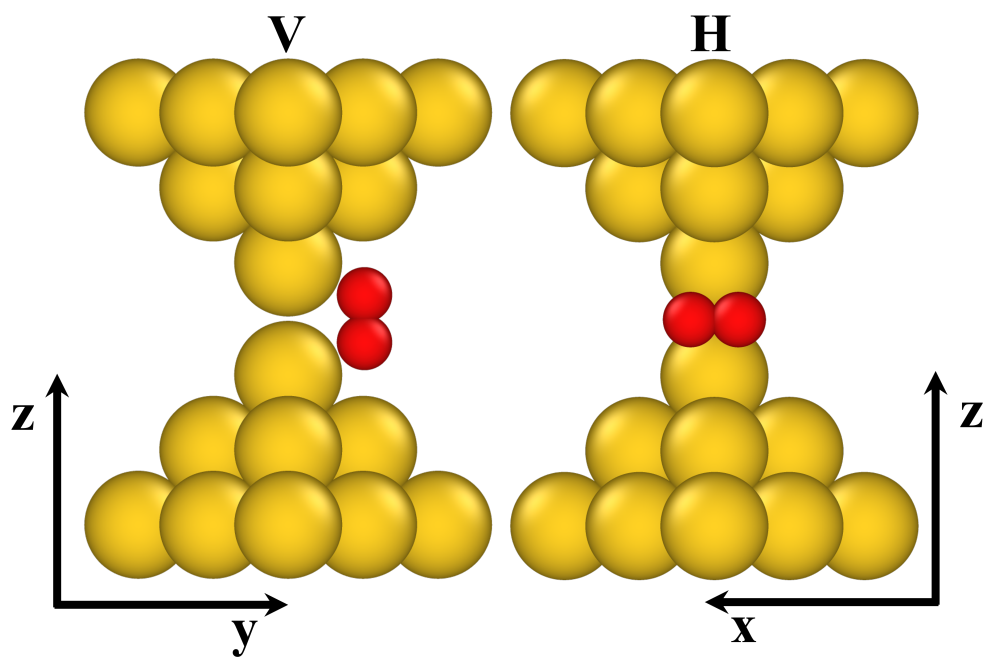


Figure S3: Schematic representation of the toy model used to estimate the MAE.